Particle sorting using a porous membrane in a microfluidic device†

Huibin Wei,[ab] Bor-han Chueh,[b] Huiling Wu,[bc] Eric W. Hall,[b] Cheuk-wing Li,[b] Romana Schirhagl,[b] Jin-Ming Lin*[a] and Richard N. Zare*[b]

Received 16th June 2010, Accepted 5th October 2010
DOI: 10.1039/c0lc00121j

Porous membranes have been fabricated based on the development of the perforated membrane mold [Y. Luo and R. N. Zare, *Lab Chip*, 2008, **8**, 1688–1694] to create a single filter that contains multiple pore sizes ranging from 6.4 to 16.6 μm inside a monolithic three-dimensional poly(dimethylsiloxane) microfluidic structure. By overlapping two filters we are able to achieve smaller pore size openings (2.5 to 3.3 μm). This filter operates without any detectable irreversible clogging, which is achieved using a cross-flow placed in front of each filtration section. The utility of a particle-sorting device that contains this filter is demonstrated by separating polystyrene beads of different diameters with an efficiency greater than 99.9%. Additionally, we demonstrate the effectiveness of this particle-sorting device by separating whole blood samples into white blood cells and red blood cells with platelets.

Introduction

Several reports exist concerning efforts to make miniaturized particle-sorting devices on a microfluidic platform. Many particle sorters use dielectrophoretic forces,[1,2] optical tweezing forces,[3,4] hydrodynamic/hydrophoretic forces,[5–8] magnetic forces,[9,10] shear-induced lift forces,[11,12] and gravity-driven forces.[13] However, many of these approaches are rather complicated, expensive, and can require additional steps to tag the particles to be sorted. Furthermore, the sorting efficiency of some of these methods is insufficient for diagnostic and therapeutic applications, such as PCR,[14,15] or early cancer detection *via* circulating tumor cells (CTCs).[16–18] The separation of particles based on size using microstructures that act as microscale filters has also been reported, and mainly belong to four types: weir-type,[19] pillar-type,[20] cross-flow,[21–23] and membrane filters.[24,25] The membrane-filter type allows for a simpler method to sort particles and cells and is the easiest to integrate into a miniaturized instrument for the rapid analysis of microlitre volumes, such as blood in point-of-care diagnostic tests.

However, the reported filters for size-based separations face the disadvantages of clogging and a relatively low sorting efficiency that can be insufficient depending on the desired use. We present an alternative method for particle sorting that uses poly(dimethylsiloxane) (PDMS) as a porous membrane to create a filter system within a monolithic microfluidic device that we believe remedies these problems. In this case, the integration of a porous PDMS membrane can be achieved without resorting to plasma oxidation, which can clog microchannels. To prepare porous PDMS membranes, SU-8 posts with controllable, variable diameters are fabricated on a silicon wafer. A thin film of PDMS is spin-coated on the wafer such that its thickness is less than the height of the SU-8 posts. The resulting thin porous PDMS film is peeled cleanly off the wafer using a specially designed cured PDMS frame.

This method[26] allows multiple pore sizes on a single membrane, in contrast to commercially available porous membranes that only have one fixed pore size. This feature allows our device to produce a series of size fractions from a whole sample within a single microdevice. Moreover, the position of the pores can be controlled by a user-designed pattern of photoresist posts, while the pores obtained on a commercial membrane are arranged randomly. The smallest pore size on a single membrane is limited by the resolution of our mask and the fidelity of our photoresist to be about 6.4 μm. Still smaller pore sizes are achieved by overlapping two membranes, as described below.

Here, we demonstrate a proof-of-concept of this device by fabricating a particle sorter that is capable of separating polystyrene microbeads of different sizes (2.5 μm to 20 μm), as well as different components of whole blood. The flow first passes through the larger pores before it passes through the smaller pores of the same membrane. For polystyrene microbeads, greater than 99.9% separation efficiency was achieved, whereas for whole blood 99.7% separation efficiency was demonstrated. We believe the simplicity of this approach makes it quite appealing, especially for being integrated into point-of-care diagnostics.

Experimental

Reagents and materials

Poly(dimethylsiloxane) (PDMS) RTV 615 was obtained from GE Silicones (Waterford, NY, USA). SU-8 negative photoresist was purchased from Microchem (Sunnyvale, CA, USA). Methyltrichlorosilane (MTS) was obtained from Sigma-Aldrich (St Louis, MO, USA). BSA and phosphate-buffered saline (PBS) were

[a]*The Key Laboratory of Bioorganic Phosphorus Chemistry & Chemical Biology, Department of Chemistry, Tsinghua University, Beijing, 100084, China. E-mail: jmlin@mail.tsinghua.edu.cn; Fax: +86-10-62792343; Tel: +86-10-62792343*
[b]*Department of Chemistry, Stanford University, Stanford, California, 94305-5080, USA. E-mail: zare@stanford.edu; Fax: +1 650 725-0259; Tel: +1 650 723-3062*
[c]*School of Pharmacy, The Second Military Medical University, Shanghai, 200433, China*

† Electronic supplementary information (ESI) available: detailed description of our device fabrication optimization experiment and data that demonstrate the reproducibility of our sorting experiments. See DOI: 10.1039/c0lc00121j

obtained from Invitrogen Corp. (Carlsbad, CA, USA), and tween-20 was purchased from Sigma-Aldrich (St Louis, MO, USA). Polystyrene (PS) latex microspheres with diameters of 2 μm and 15 μm were manufactured by Invitrogen Corp. (Carlsbad, CA, USA) and PS 20 μm microspheres were obtained from Polysciences Inc. (Warrington, PA). SPR 220-7 positive photoresist, hexamethyldisilazane (HMDS), and photoresist-developing reagents SU-8 Developer and MF-26A solvent are common chemicals provided by the Stanford Nanofabrication Facility.

Whole mouse blood, which was collected from just-born female white mice, and human leukemia (REH) cells were obtained from the Stanford School of Medicine.

The integrated particle sorter device

Our idea of fabricating a porous membrane by using the photoresist posts on a wafer is based on previous work in the Zare laboratory.[26] We have improved upon this work by using photoresist posts with greatly decreased diameters and a reusable mold. There are many commercial porous membranes produced that can achieve sizes into the nanometre scale. However, this option allows for only one size of pore on a single membrane and the pores are arranged randomly. Here we describe a porous PDMS membrane in which the pores are arranged in a specific pattern and can be designed and produced in different sizes on a single membrane. This last feature allows us to use the same membrane within a device to sort and collect different fractions of particles based on size.

Fig. 1 shows schematics of our microfluidic device that is capable of sorting particles with three different diameters. Each filtering step is performed within an assembly of two chambers sandwiching a section of the porous membrane (Fig. 1A, inset shows a membrane with 6.4 μm pores). The chambers have a rounded cross-section because their molds were fabricated from positive photoresist that was reformed *via* post-development baking, which is explained in more detail below. Our integrated particle-sorting device contains two such assemblies. The analyte stream first flows from the bottom chamber to the top chamber in the first assembly, which contains the section of the membrane with the larger pores. This removes the largest particles from the stream. The stream then moves to a second assembly, where it flows from a second top chamber to another bottom chamber through the section of the membrane with the smaller pores (Fig. 1B), thus separating the particles of intermediate and smallest size from each other.

The flow channels have smooth curved surfaces derived from reshaped photoresist, which will be described later, while the valve channels are cast from rectangular photoresist. Normally, flow and valve architectures are maintained on separate layers. However, in our work we require a 3D microfluidic structure in which a porous membrane is sandwiched between two flow layers, so a much longer interconnection between the valves and their inlets would have been necessary were the normal valve design methodology adopted. A longer interconnection would introduce more resistance and thus require higher pressure to close the valves, which would cause more problems during chip operation. To solve this problem, we developed a three-state valve (Fig. 1C) to reduce the interconnection inside the 3D channel-valve microstructure. In this case, flow channels and

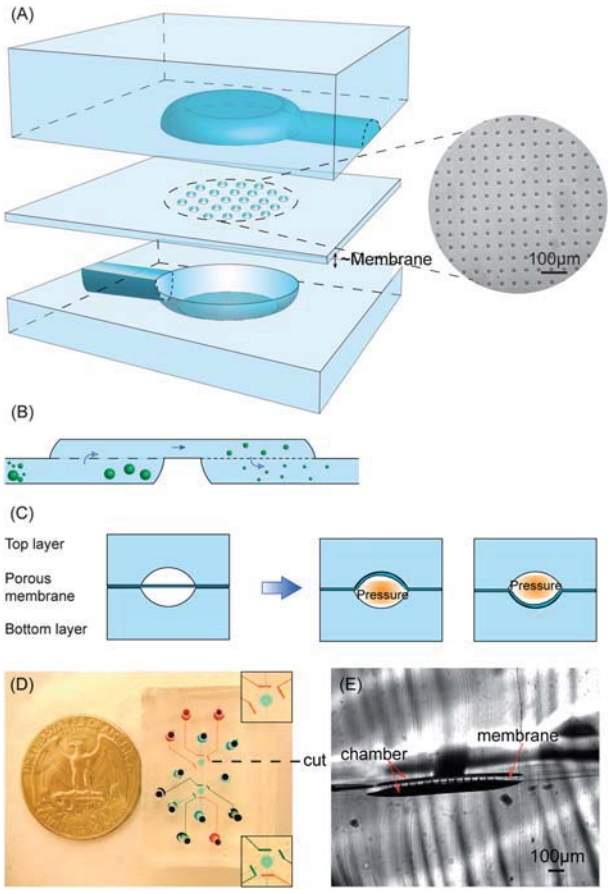

Fig. 1 (A) Partial scheme of the 3D particle sorter. The inset shows the image of the porous membrane obtained under an optical microscope. (B) Scheme of the sectional view of the particle sorter. (C) Schematic illustration of the three-state valve. The valve could close either the top channel or bottom channel, as determined by which layer is pressurized. (D) Picture of the three-size particle sorter. The insets show enlarged images of the two chamber areas. (E) Image of the cross-section along dashed line of (D).

valve channels were fabricated on the same positive resist mold, allowing for a simpler design that incorporates less interconnection and gives both flow and valve architecture a rounded cross-section. The porous PDMS membrane sandwiched between the two layers doubles as the thin film for closing a flow channel as a valve. The membrane is not porous in these areas.

Fig. 1D shows a picture of a fabricated particle sorter. Channels filled with blue dye represent the flow channels, interconnected across layers to form a 3D structure. Channels filled with red and green dyes are valves which, as stated above, are fabricated in the top and bottom flow layers, respectively. A scalpel was used to cut through the chamber along the dashed line, and the cross-section was examined under an optical microscope. In Fig. 1E, the through-pores and the PDMS membrane layer can be clearly seen between the two flow layers. The streaks on the images are caused by mechanical cutting from the scalpel.

Fabrication of soft lithography molds

Each PDMS layer was individually fabricated using a specific mold, which in turn was produced on a silicon wafer *via* standard

photolithography techniques in the Stanford Nanofabrication Facility. The patterns for this architecture were printed on transparency masks at a resolution of 40 640 dpi from Fineline Imaging (Colorado Springs, CO, USA). In this work, there were two types of silicon wafer molds: the mold for the porous membrane (POM-mold) and the molds for the flow layers. With regard to the POM-mold, it should be noted that in order to form complete pores, the height of the SU-8 posts must be greater than the desired thickness of the PDMS porous membrane.

To fabricate the POM-mold, SU-8 2015 photoresist was spin-coated on an HMDS-primed silicon wafer at a thickness of 20 μm and baked at 95 °C for 4 min. The photoresist on the silicon wafer was exposed under UV light through a transparency mask and baked at 95 °C for 5 min, and developed with SU-8 Developer. Optimization procedures for the POM-mold are described in the ESI†. To fabricate the flow-layer molds, SPR 220-7 photoresist was spin-coated on an HMDS-primed silicon wafer at a thickness of 20 μm and 30 μm, respectively, for the top and bottom flow layers, then baked at 95 °C for 200 s. The photoresist on the silicon wafer was exposed under UV light through a transparency mask and developed in MF-26A solvent. The flow-layer molds were baked on a hot plate (120 °C for 8 min) to give the photoresist architecture a more rounded cross-section, which facilitates more complete valving of the resulting PDMS channels.[27] Prior to use in soft lithography, all molds were exposed to MTS vapor in a vacuum desiccator in order to prevent adhesion between the cured PDMS and the mold. The flow layer molds were exposed to MTS for 30 min, while the POM-mold was exposed for 4 h to achieve a more hydrophobic surface around the posts.

Fabrication of the 3D microfluidic device

The microfluidic particle sorter was assembled in-house in the Zare lab from three sections: the top flow layer, the membrane layer, and the bottom flow layer. The top and bottom flow layers were both fabricated as PDMS slabs with thicknesses of 7 mm and 2 mm, respectively, while the membrane layer was a thin PDMS film with a thickness of less than 20 μm. Optimization of the cyclohexane dilution and spin-coating speed used to fabricate the membrane are described in the ESI†. An imbalanced cross-linking ratio bonding method[28] was adopted in our experiments because successful alignment of the layers required a low error tolerance, and this method allowed us to continually correct alignment. The principle of imbalanced cross-linking ratio bonding is based on the theory that the cross-linking agent can migrate through the interface between cross-linker-poor and cross-linker-rich layers. All layers to be aligned are cured into a solid state that can easily be removed from the molds. Despite their cured nature, the layers retain a sufficient imbalance with regard to their cross-linked state such that an effective bond can form between them at their interface. Thus, the imbalanced cross-linking ratio bonding method allows for multiple alignment attempts, because both layers are solid, without damaging either layer.

The fabrication process is described as follows:

(1) Well-mixed liquid PDMS prepolymer was poured onto the molds of the top and bottom flow layers. The prepolymer for the top flow layer was mixed with an excess of cross-linker (mass ratio 5 : 1 RTV A : B), while the prepolymer for the bottom layer was mixed with a deficiency (mass ratio 20 : 1 RTV A : B). After degassing both layers under a vacuum, they were cured in an 80 °C oven for 1 h.

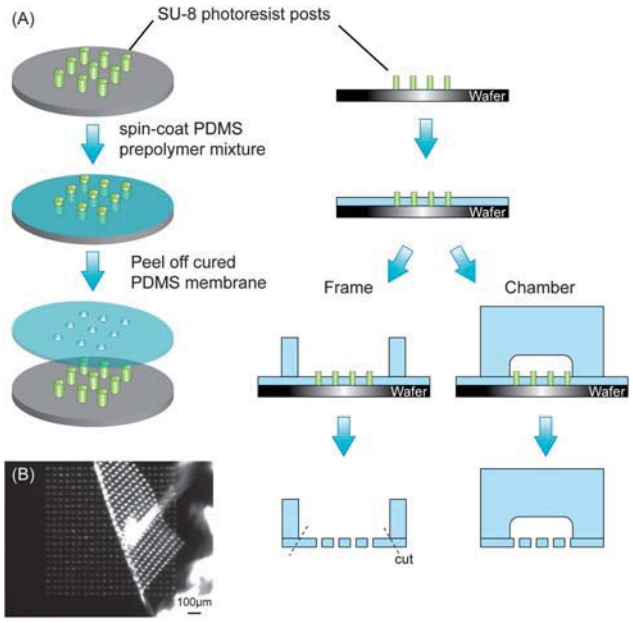

Fig. 2 (A) Schematic of the procedure for making a porous PDMS membrane from the POM-mold. Illustration of the cross-section is presented on the right. (B) Image of the porous PDMS membrane being peeled from the POM-mold.

(2) The cured PDMS slabs (the top layer was 7 mm and the bottom layer was 2 mm) were cut with a scalpel and peeled from the mold. Holes were punched through the channel inlets of the top flow layer with a syringe needle that had the tip sawed off.

(3) A 10 : 1 mass ratio of PDMS was diluted in a one-half mass equivalent of cyclohexane. The mixture was spin-coated on the POM-mold with an initial spin rate of 500 rpm for 18 s and a final spin rate of 3000 rpm for 60 s. The mold was placed on a flat surface at room temperature for 40 min to allow the surface of the PDMS to smoothen, and then inserted into an 80 °C oven for 20 min to cure the membrane layer.

(4) The top flow layer prepared in Step 2 was placed on the PDMS-coated POM-mold and aligned by inspection through a stereoscope (Fig. 2). Afterwards, a 5 : 1 PDMS prepolymer mixture was poured around the aligned layers and then cured at 80 °C for 1 h.

(5) The chips were cut from the POM-mold. Access holes were punched through the combined layers at positions corresponding to the inlets and outlets of the bottom flow layer.

(6) The resulting chips in Step 5 were placed on the bottom flow layer prepared in Step 1, aligned by inspection, and sealed with gentle pressure. The whole device was placed in an 80 °C oven overnight for final bonding.

Samples and setup

Whole mouse blood was collected from white mice into Microtainer tubes containing dipotassium EDTA (Fisher Scientific, Montreal, QC, USA). Blood samples were used within 1 d of

collection. The REH human leukemia cell lines were grown in RPMI 1640 medium (Invitrogen) supplemented with 10% fetal bovine serum, 25 mM HEPES and L-glutamine in an incubator maintained at 37 °C with 5% CO_2. The REH cells used in the experiment were obtained after 3–4 days of culturing, which had a rough concentration of 10^6 μL^{-1}. The whole blood sample was diluted by a factor of 40 in PBS buffer. REH cell suspension was mixed with diluted whole blood in a 1 : 1 ratio before injection into the particle sorter.

Integrated microfluidic devices were filled and flushed with 0.2% (v/v) aqueous solution of tween-20 before loading the PS beads and 1% (w/v) BSA solution in PBS buffer before loading blood samples. Sample mixtures were introduced from the inlet, and moved along the channels using a homemade pressure controller in the Zare lab. A microscope (Nikon ECLIPSE TE2000-U, Kanagawa, Japan) equipped with a CCD camera (Mintron MTV-63KR11N, Fremont, CA, USA) was used to observe and obtain images of the microfluidic device. Upon completion of separation, the samples were collected at the different outlets by gel-loading pipet tips, diluted with the Isoton diluent (Beckman Coulter Inc., Brea, CA, USA), and further analyzed for enumeration and size distribution measurements using a Coulter counter (Model Z2, Beckman Coulter Inc.) located in the Stanford School of Medicine (Stanford, CA, USA).

Results and discussion

Aligned overlap of porous membranes for the fabrication of smaller pores

It is possible to create even smaller pores within a PDMS membrane than those described above by aligning two porous membranes such that their pores overlap. The size of the overlap determines the size of the new, smaller pore. This was accomplished in the following manner (Fig. 3). Membrane 1 was formed from a PDMS prepolymer, mixed in 5 : 1 mass ratio and then diluted in cyclohexane by a factor of 2. Because the viscosities of PDMS RTV A and B are similar, this ratio adjustment did not cause any apparent change to the membrane thickness from the results obtained previously. Following curing at 80 °C, a PDMS frame was used to peel off porous membrane 1 from the POM-mold. The membrane was carefully placed onto a pre-cleaned glass slide with care to prevent trapping air

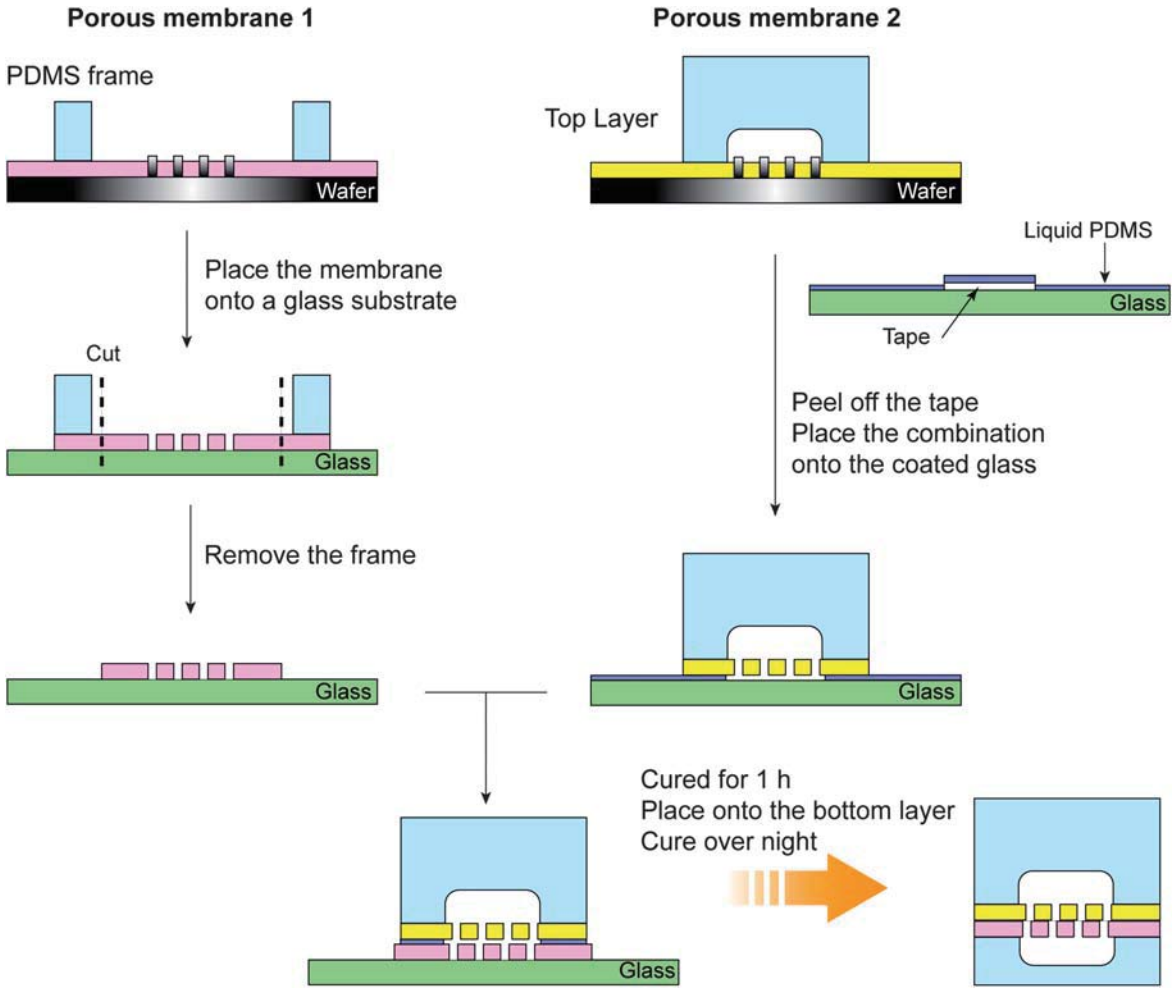

Fig. 3 Schematic of the fabrication procedure for the overlapped aligned porous membrane. Different PDMS membranes are labeled with different colours.

between the membrane and the glass slide. Due to electrostatic interaction, the thin film tightly attached to the glass surface. A scalpel was used to remove the PDMS frame and the redundant film on the edges of porous membrane 1. Meanwhile, porous membrane 2 was bound to the top flow layer according to the procedures described above for fabrication of a single porous membrane.

The two porous PDMS membranes were bound by the dipping–attaching method, as described elsewhere.[29,30] Briefly, PDMS prepolymer (mixed in a 10 : 1 mass ratio), diluted in cyclohexane by a factor of 3, is spin-coated on a glass slide at 3300 rpm to form a thin film. To form an even thinner film, the glass slide is put into an 80 °C oven to cure for 2 min before it was used. A PDMS layer is then dipped into the mortar and attached to another PDMS layer. Thus, between the two PDMS layers a portion of the thin film of PDMS prepolymer is present, which is then cured in an oven at 80 °C for 1 h to become an adhesive PDMS layer.

However, for the porous PDMS membrane, the normal dipping–attaching method is not applicable because the size of the pores is so small that the mortar clogs the pores when the membrane is dipped into it. To prevent pore clogging, a partially "mortar-free" method was introduced for bonding two porous PDMS membranes. A small piece of tape, which was slightly larger than the chamber on the top flow layer, was pasted onto a specific position of the glass slide, corresponding to the position of the chamber on the top flow layer. After spin-coating the PDMS prepolymer solution, and curing in the oven, the cover tape was peeled off, leaving that space free of mortar. Following alignment of the top chamber layer to porous membrane 2, the combined PDMS structure was dipped into the mortar such that the mortar-free area was located under the chamber. The combined structure was then aligned and bound to porous membrane 1 prior to curing it in an 80 °C oven for 1 h. The whole device was finished by bonding the resulting three layers with the bottom flow layer by curing the entire chip in an 80 °C oven overnight.

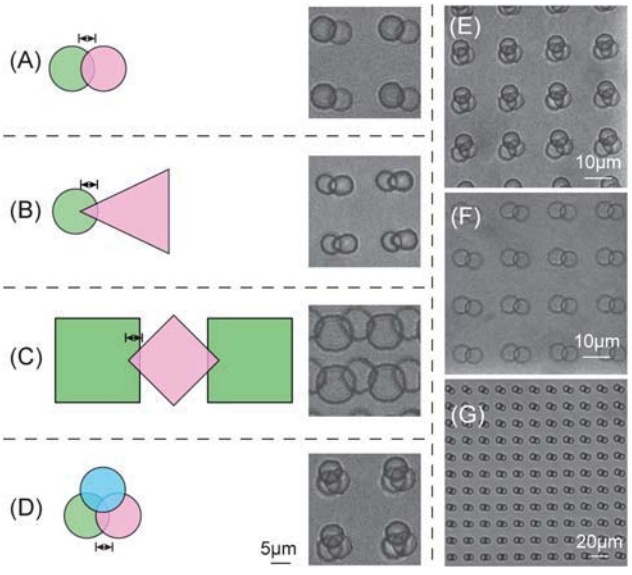

Fig. 4 (A–D) Schematic illustrations of the expected pore shapes are shown in the left column, while microscopic images of the overlapped aligned porous membranes are shown in the right column. (E and F) Microscopic images of the overlapped pore array. (G) Microscopic images of the overlapped pore array showing a larger area.

Fig. 4 shows a schematic illustration and microscopic images of the aligned, overlapped porous membrane. Taking the overlapped pores in Fig. 4B as an example, an overlapping area with a diameter ranging between 2.5 μm and 3.3 μm was created. Additionally, three-layer overlapped pores were achieved according to the same procedures, as shown in Fig. 4D. Due to the resolution limitations of the mask, no sharply angled shapes could be fabricated for the pores on the membrane. The production of triangular- and rectangular-shaped pores exhibited rounded corners instead of sharp angles. The error in the size of the smaller, overlapped pore that is created as a result of this process has not yet been characterized. Regardless, we have demonstrated a novel, relatively cheap and surprisingly simple method of fabricating customizable PDMS membranes for use in a monolithic particle-sorting device. As an aside, one may avoid cells and particles becoming trapped between the membranes *via* frequent 'flush-and-collect' cycles, as well as treating the surface with polyvinyl acetate in the case of cells to avoid adhesion.

Particle sorting process

A. Polystyrene microbeads. To demonstrate the effectiveness of the particle sorter, we tested the separation of polystyrene beads with different diameters as a proof-of-concept. PS beads with diameters of 2.5 μm, 15 μm, and 20 μm were mixed in a 0.2% tween-20 solution for evaluation of the device's sorting efficiency. For this demonstration, a device was fabricated in which the membrane contained 16.6 μm pores in the first assembly and 6.4 μm pores in the second. Fig. 5 illustrates the sorting procedure. The chip consists of two sections: the main flow channel (straight channel with valves 1, 4, 7 turned off) and the flushing channels (beveled channels with valves 2, 3, 5, and 6 turned on). Valves 1, 2, 3, and 7 are on the top layer and valves 4, 5, and 6 are on the bottom flow layer.

In our device, sorting particles is a two-step process. First, the particle suspension is introduced into the inlet with a pressure of 10 psi. Particles are directed though the main flow channel because valves 2, 3, 5, and 6 are closed. When the mixture meets the first chamber, the 20 μm particles are blocked by the porous membrane and gather in the bottom layer, while the 15 μm and 2.5 μm particles go through the pores and continue flowing in the channel on the top flow layer. The 15 μm particles are then trapped in the second chamber on the top flow layer while the 2.5 μm particles are collected at the end of the main flow channel on the bottom layer. Second, the device is reconfigured for collection of particles by closing valves 1, 4, and 7 and opening valves 2, 3, 5, and 6. A 0.2% tween-20 solution is injected into the beveled channels to flush the 15 μm and 20 μm particles to the outlets in order to collect them. New samples can then be injected to continue sorting. To prevent the generation of air bubbles, the channels were filled with deionized water containing 0.2% tween-20 prior to the sorting process.

Irreversible clogging was successfully avoided by flushing the chamber and collecting the samples frequently. A few cells stick to the membrane but are easily removed on further flushing. The separation efficiency of the separated sample was defined as the

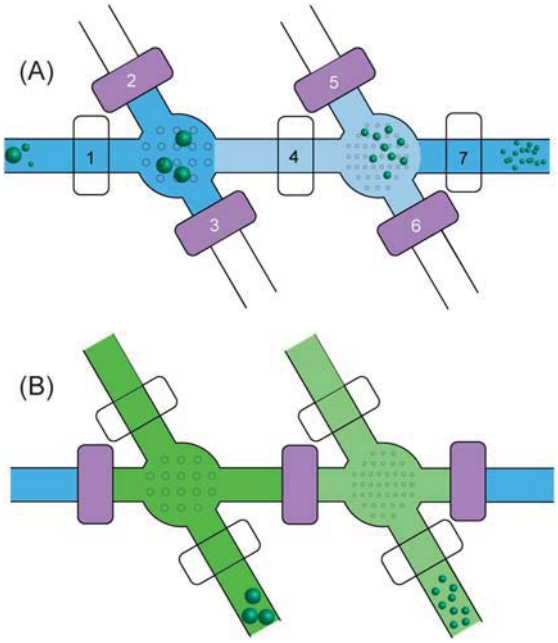

Fig. 5 Procedure for sorting particles with three different diameters. The darker color represents liquid flow in the bottom layer; the lighter color represents liquid flow in the top flow layer.

ratio of the number of particles with a diameter inside the target size range to the total number of particles collected. The size distribution measurements from the Coulter counter (Fig. 6) revealed that the separation efficiency of separated samples in each collector was greater than 99.9%, as determined from the data output from the Coulter counter. This experiment was repeated 15 times.

B. Whole blood cells. Whole blood cells were obtained to evaluate the efficiency of sorting particles within a biologically relevant sample. Please note that white blood cells are at a concentration one-thousandth of that of red blood cells, so their number was supplemented with similar-sized REH cells so that the separation of the two differently sized groups could be more precisely evaluated.

White blood and REH cells were separated from whole blood by moving them through a porous membrane with a pore size of 6.4 μm. Because red blood cells have a disk diameter of 4–5 μm, and white blood cells and REH cells have a diameter of 7–10 μm (Fig. 7D), the white blood and REH cells were blocked while the red blood cells and platelets went through the pores to be collected at the outlet. For each separation experiment, 10 μL samples were loaded. Approximately 10^7 cells were sorted in each separation that had the duration of 3–5 min. Fig. 7 presents the sorting results evaluated *via* a Coulter counter. The mean diameter was 5.982 μm, and ~40% of the cells had a diameter larger than 6.4 μm. Following separation, size measurements of the purified sample that contained cells with a diameter less than 6.4 μm had a separation efficiency greater than 99.9% and a mean diameter of 4.056 μm (Fig. 7B). The purified sample that contained cells with a diameter greater than 6.4 μm was found to have a separation efficiency of 99.7% and a mean diameter of

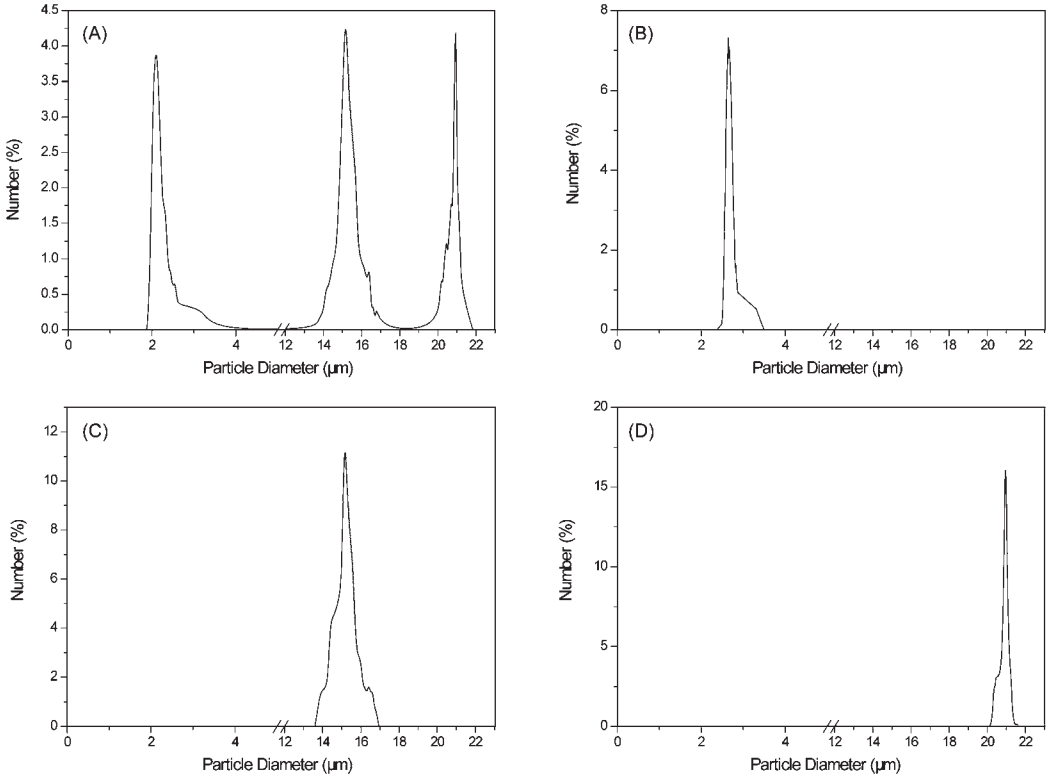

Fig. 6 Sorting results for different sizes of PS particles. (A) Particle mixture measurement before sorting; (B), (C), and (D) measurement of the smallest, intermediate and largest collected particles, respectively.

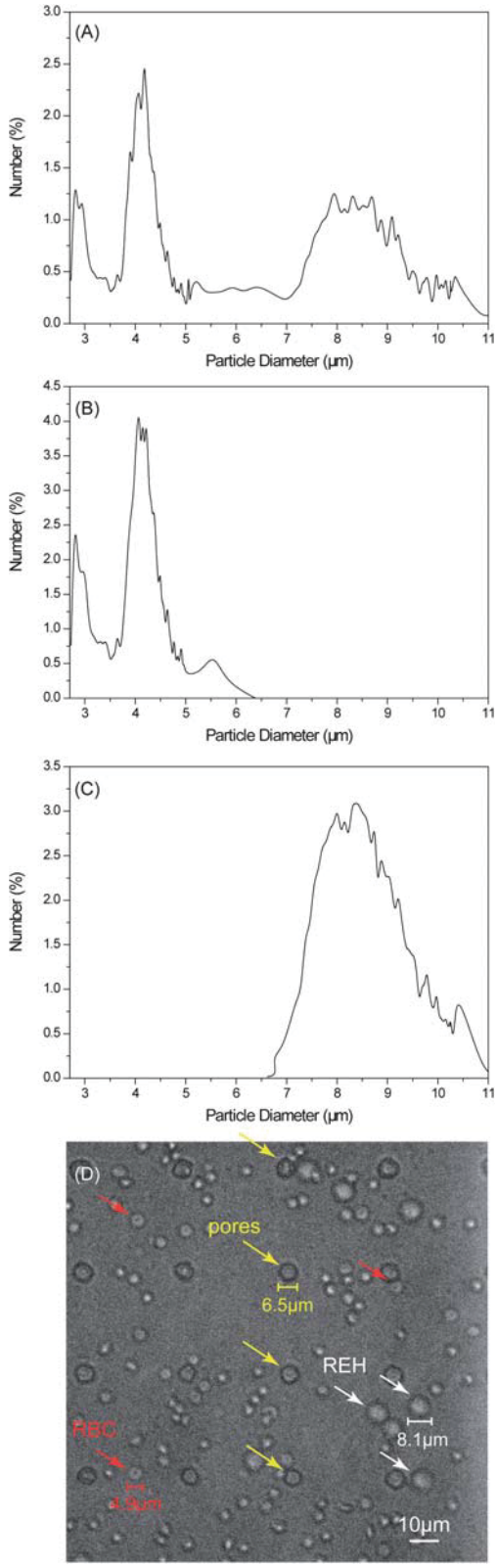

Fig. 7 Sorting results of whole blood. (A) Particle distribution measurements of whole blood before sorting; (B) particle distribution measurements of collected red blood cells and platelets; and (C) collected white blood cells and REH cells. (D) Microscopic images inside the sorting chamber. Red arrows point at red blood cells (RBC) and yellow arrows point to REH cells, respectively.

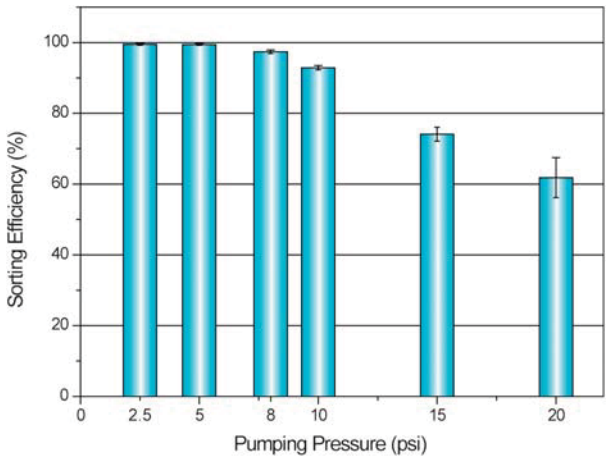

Fig. 8 Plot of sorting efficiency *versus* driving pressure. A 99.7% sorting efficiency could be achieved at or below a pressure of 5 psi. A poor efficiency was observed for pressures at or above 15 psi.

8.688 μm (Fig. 7C). This experiment showed good reproducibility (Fig. S2†). The whole device was treated with 1% (w/v) BSA solution in PBS before loading the blood samples to avoid adhesion to the channel wall. The viability of cells was qualitatively confirmed to remain high following the sorting process (Fig. S4†). Irreversible clogging was prevented by flushing the filter chamber after every separation and collection cycle (Fig. S3†).

While a stronger driving pressure will produce a faster separation, it will also result in a poorer sorting efficiency caused by the increased flexibility of cells compared to the polystyrene beads. We evaluated and optimized the influence of increased driving pressure on the sorting efficiency. Fig. 8 shows this relationship. The data show that with a pushing pressure of less than 5 psi, 99.7% sorting efficiency was achieved. When the driving pressure was increased to 8 psi, the sorting efficiency decreased to 97.4%. The drop in efficiency became more dramatic as the driving pressure was increased beyond 10 psi. In order to maximize sorting speed without significantly sacrificing sorting efficiency, a driving pressure of 5 psi is suggested.

Conclusions

In this paper, we have described a microfluidic particle sorter which incorporates a PDMS porous membrane. Membranes containing pores as small as 6.4 μm were easily fabricated on a POM-mold, and even smaller pores were generated by aligning two or more membranes so that the pores overlapped. A sorting efficiency greater than 99.9% for polystyrene beads and a 99.7% sorting efficiency for whole blood were achieved from our particle sorter. We were able to separate white blood cells, as well as red blood cells and platelets combined, from whole blood. Additionally, the size of the pores could be conveniently changed to fit the specific objective, such as CTCs. We believe that these results demonstrate the potential of this simple monolithic microfluidic particle sorter to be integrated in miniaturized and automatic equipment for point-of-care diagnostics. Further work is needed to perfect this setup for isolation, collection, and

enumeration of blood components, but the present results clearly demonstrate the principles of this new separation device.

Acknowledgements

H. Wei acknowledges the China Scholarship Council ([2009]3003). This work was supported by National Natural Science Foundation of China (Nos. 20935002, 90813015) and the US National Science Foundation (NSF-BSC 0636284). The authors would also like to acknowledge the support and expertise of the staff of the Stanford Nanofabrication Facility.

References

1 M. Durr, J. Kentsch, T. Muller, T. Schnelle and M. Stelzle, *Electrophoresis*, 2003, **24**, 722–731.
2 D. Chen and H. Du, *Microfluid. Nanofluid.*, 2007, **3**, 603–610.
3 C. C. Lin, A. Chen and C. H. Lin, *Biomed. Microdevices*, 2008, **10**, 55–63.
4 J. Prikulis, F. Svedberg, M. Käll, J. Enger, K. Ramser, M. Goksor and D. Hanstorp, *Nano Lett.*, 2004, **4**, 115–118.
5 S. Choi, S. Song, C. Choi and J. K. Park, *Lab Chip*, 2007, **7**, 1532–1538.
6 M. Hashimoto, P. Garstecki and G. M. Whitesides, *Small*, 2007, **3**, 1792–1802.
7 M. Yamada and M. Seki, *Anal. Chem.*, 2006, **78**, 1357–1362.
8 M. Yamada, M. Nakashima and M. Seki, *Anal. Chem.*, 2004, **76**, 5465–5471.
9 J. H. Kang and J. K. Park, *Small*, 2007, **3**, 1784–1791.
10 K. E. McCloskey, J. J. Chalmers and M. Zborowski, *Anal. Chem.*, 2003, **75**, 6868–6874.
11 D. Di Carlo, D. Irimia, R. G. Tompkins and M. Toner, *Proc. Natl. Acad. Sci. U. S. A.*, 2007, **104**, 18892–18897.
12 D. Di Carlo, J. F. Edd, D. Irimia, R. G. Tompkins and M. Toner, *Anal. Chem.*, 2008, **80**, 2204–2211.
13 D. Huh, J. H. Bahng, Y. Ling, H.-H. Wei, O. D. Kripfgans, J. B. Fowlkes, J. B. Grotberg and S. Takayama, *Anal. Chem.*, 2007, **79**, 1369–1376.
14 J. Cheng, L. J. Kricka, E. L. Sheldon and P. Wilding, in *Microsystem Technology in Chemistry and Life Sciences*, 1998.
15 P. Wilding, L. J. Kricka, J. Cheng, G. Hvichia, M. A. Shoffner and P. Fortina, *Anal. Biochem.*, 1998, **257**, 95–100.
16 J. Li, Z. Zhang, J. Rosenzweig, Y. Y. Wang and D. W. Chan, *Clin. Chem. (Washington, DC, U. S.)*, 2002, **48**, 1296–1304.
17 J. Villanueva, D. R. Shaffer, J. Philip, C. A. Chaparro, H. Erdjument-Bromage, A. B. Olshen, M. Fleisher, H. Lilja, E. Brogi, J. Boyd, M. Sanchez-Carbayo, E. C. Holland, C. Cordon-Cardo, H. I. Scher and P. Tempst, *J. Clin. Invest.*, 2006, **116**, 271–284.
18 M. Cristofanilli, G. T. Budd, M. J. Ellis, A. Stopeck, J. Matera, M. C. Miller, J. M. Reuben, G. V. Doyle, W. J. Allard, L. W. Terstappen and D. F. Hayes, *N. Engl. J. Med.*, 2004, **351**, 781–791.
19 V. VanDelinder and A. Groisman, *Anal. Chem.*, 2006, **78**, 3765–3771.
20 H. Mohamed, J. N. Turner and M. Caggana, *J. Chromatogr., A*, 2007, **1162**, 187–192.
21 P. Sethu, A. Sin and M. Toner, *Lab Chip*, 2006, **6**, 83–89.
22 V. VanDelinder and A. Groisman, *Anal. Chem.*, 2007, **79**, 2023–2030.
23 S. Murthy, P. Sethu, G. Vunjak-Novakovic, M. Toner and M. Radisic, *Biomed. Microdevices*, 2006, **8**, 231–237.
24 H. Ji, V. Samper, Y. Chen, C. Heng, T. Lim and L. Yobas, *Biomed. Microdevices*, 2008, **10**, 251–257.
25 S. Zheng, H. Lin, J. Liu, M. Balic, R. Datar, R. J. Cote and Y. Tai, *J. Chromatogr., A*, 2007, **1162**, 154–161.
26 Y. Luo and R. N. Zare, *Lab Chip*, 2008, **8**, 1688–1694.
27 V. Studer, G. Hang, A. Pandolfi, M. Ortiz, W. F. Anderson and S. R. Quake, *J. Appl. Phys.*, 2004, **95**, 393–398.
28 M. A. Unger, H.-P. Chou, T. Thorsen, A. Scherer and S. R. Quake, *Science*, 2000, **288**, 113–116.
29 H. Wu, B. Huang and R. N. Zare, *Lab Chip*, 2005, **5**, 1393–1398.
30 Y. Luo, F. Yu and R. N. Zare, *Lab Chip*, 2008, **8**, 694–700.